POLITECNICO DI TORINO
Repository ISTITUZIONALE

Numerical analysis of process-induced deformations and stresses in aeronautical composite
components

(Article begins on next page)

21 December 2024

NUMERICAL ANALYSIS OF PROCESS-INDUCED DEFORMATIONS AND STRESSES IN AERONAUTICAL COMPOSITE COMPONENTS

Rebecca Masia[1], Marco Petrolo[1], Enrico Zappino[1], Navid Zobeiry[2] & Erasmo Carrera[1]

[1]MUL2 Lab, Department of Mechanical and Aerospace Engineering, Politecnico di Torino, Turin, Italy
[2]Materials Science & Engineering Department, University of Washington, Seattle, USA

Abstract

Process-Induced Deformations (PIDs) pose notable challenges in fabricating composite aerostructures, particularly during the alignment phase of wing spars and skins in composite wing boxes. The present study explores the effects of design and geometric variables on PIDs and their consequent residual stresses within composite spars. The focus will be on components with C-shaped cross-sections, examining factors such as spring-in angles, deformations, and the distribution of 3D stresses throughout the thickness of these components. The research utilizes one-dimensional, higher-order, layer-wise theories derived from the Carrera Unified Formulation (CUF) to overcome the traditionally time-consuming simulations for such large geometries. The cure-hardening instantaneously linear elastic (CHILE) model will be adopted for the numerical simulation. The present methodology facilitates a swift and effective assessment of residual stresses and PIDs, enabling prompt evaluation of various design options. This tool is particularly advantageous for exploring and optimizing designs of large and complex composite components and devising strategies to reduce the impact of PIDs.

Keywords: Virtual manufacturing, Composites, CUF, Defects

1. Introduction

Composite materials are common in developing high-performance structural elements within the aviation sector [1]. The unique combination of exceptional rigidity, tensile strength, and lightweight properties makes carbon fiber-reinforced polymers a leading material in modern engineering designs.

The production of polymer-based aerostructures presents significant challenges, such as dimensional and shape changes during curing processes [2]. These changes are critical for the structural integrity and functional performance of aeronautics components and for the assembly process of composite airframes. The complexity of an aerostructure's geometry further complicates this issue, which has become increasingly relevant due to the advanced and varied applications of composite materials in contemporary aeronautics.

Accurately predicting and controlling residual defects are paramount in manufacturing composite components, particularly those used as shear webs in aircraft wings. These components must adhere to stringent dimensional standards for proper coupling and withstand significant loads. In recent years, there have been increasing efforts in research to predict and minimize the stresses and deformations induced during manufacturing. The adoption of numerical simulations has become essential, saving time and resources while improving the accuracy of these forecasts; this is particularly critical given the increasing complexity of the components under study, such as L-C-Z-shaped models [3, 4, 5], requiring more advanced simulation methods. Recent studies have considered these configurations using both analytical and numerical techniques. A major hurdle in addressing process-induced deformation is modeling the through-the-thickness behavior, where traditional numerical models often underperform. Therefore, three-dimensional modeling becomes indispensable in simulations to accurately represent process-induced variations, ensuring the components meet the rigorous standards for their critical role in aircraft wing structures.

This study aims to advance the understanding of process-induced deformations and stresses in C-shaped composite components via one-dimensional models to improve the numerical efficiency and obtain 3D-like accuracy.

2. Numerical simulation of curing

The numerical simulation of the curing process employs the Cure-Hardening Instantaneously Linear Elastic (CHILE) model [6]. This model operates on the premise that the material's response is instantaneously linear and elastic.

The numerical procedure for the curing cycle is shown in Fig. 1. The simulation initiates at the
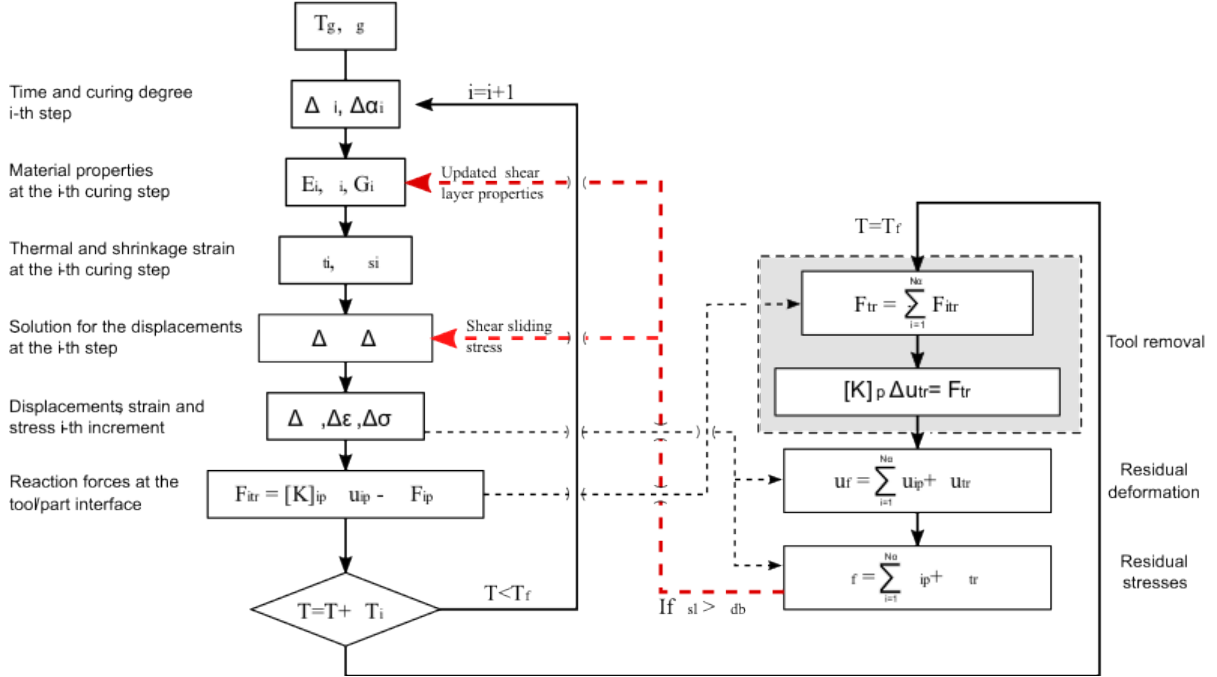

Figure 1 – Flowchart of the curing cycle numerical analysis.

gelation point and progresses iteratively. Throughout each step of the analysis, an update in the composite material's elastic, thermal, and chemical characteristics is applied. Simultaneously, the external conditions of the autoclave environment are replicated for the duration of the curing process [7]. The simulation captures the incremental displacement at each step. The final solution is derived from the aggregated total of these cumulative elastic responses for each corresponding step in the process, i.e.:

$$u = \sum_{i=1}^{N} \Delta u_i \tag{1}$$

where u is the cumulative displacement, and Δu_i denotes the incremental displacement at each step i. N is the total number of steps of the curing cycle. The simulation encompasses the component's removal from the mold, during which the force exerted between the part and the mold is stored and then applied to the part in the simulation.

The curing cycle parameters used in the simulation include an initial heating phase at a rate of 1 °C per minute, followed by a constant temperature phase at 180 °C lasting for 120 minutes, and concludes with a cooling phase. The entire cycle spans an estimated duration of about 333 minutes.

The Carrera Unified Formulation (CUF) [8, 9, 10] is employed to formulate an advanced beam theory. The CUF framework allows for a compact modeling of the three-dimensional displacement field,

$$\boldsymbol{u}(x,y,z) = F_\tau(x,z)N_i(y)\boldsymbol{u}_{\tau i} \tag{2}$$

where τ is the expansion function index, and i is the index over the 1D finite element nodes. The employed expansion functions, F_τ, are based on Lagrange polynomials, leading to a layer-wise model.

The model utilizes quadratic nine-node Lagrange elements (L9) for the cross-section and cubic four-node elements (B4) for the one-dimensional direction. Following the derivation of the displacement field, stresses are computed using Hooke's law. The problem's governing equations are formulated using the Principle of Virtual Displacements (PVD). The solutions are obtained by assembling the Fundamental Nuclei (FN) according to the CUF,

$$k^{ij\tau s} = \int_V \left[N_j F_s \boldsymbol{D}^T \boldsymbol{C} \boldsymbol{D} F_\tau N_i \right] dV \tag{3}$$

where $\boldsymbol{D}$ is the 3×6 differential operator and C is the 6×6 matrix of the elastic coefficients.

3. Component's geometry and material

Hexcel's AS4/8552 unidirectional prepreg is the material used. The cured ply of this prepreg is roughly 0.19 mm thick, comprising approximately 35% 8552 epoxy resin system by weight [11] and 65% AS4 HexTow carbon fibers with an Aerial weight of 190gsm [12] by weight. The tool is made of Invar, known for its isotropic mechanical properties, with an alpha value of 1.56E-6 /°C. A C-shaped model was retrieved from [13], comprising eight layers and symmetrical and balanced cross-ply laminations.

Figure 2 depicts the C-shaped model's geometry and reference system. The multi-layered composite model has a total thickness of 1.6 mm atop an 8 mm thick tooling base, with an intermediate shear layer one-tenth the thickness of the laminate. The entire component features one 40 mm segment parallel to the z-axis and another 100 mm long parallel to the x-axis, connected by a curved segment with external and internal radii of 14.76 mm and 5 mm, respectively. The model extends 115 mm along the y-axis, and due to symmetry, only a quarter of it is studied; the tool is simply supported.
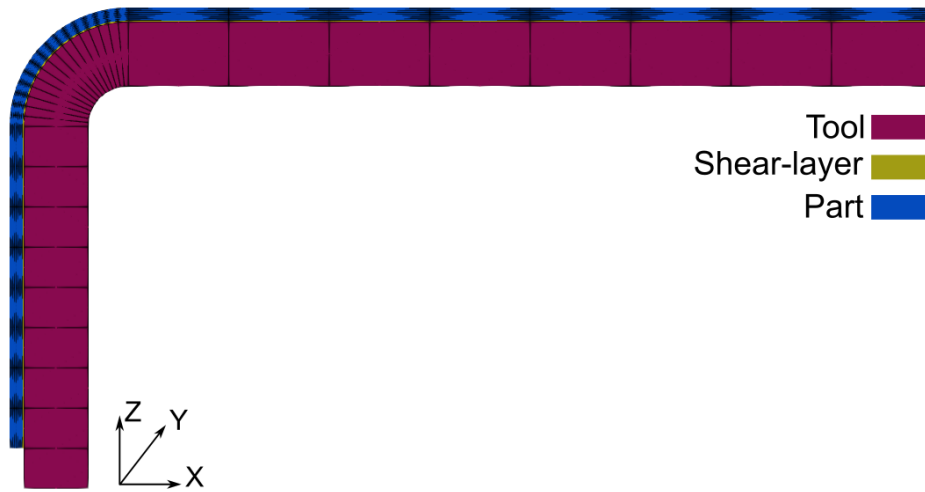

Figure 2 – C-shaped model composed by tool, shear-layer and composite part.

4. Numerical results and discussion

The numerical results focus on deformations and stresses in the cured component; symmetric and balanced cross-ply stacking sequences are considered. The primary metric for evaluating these deformations is the spring-in angle, which is crucial for ensuring compatibility with other components during the assembly phase, see Fig. 3. Furthermore, the current analysis examines the stress distribution throughout the model's thickness.

The numerical model of the C-shaped component is constructed using 321 L9 elements in the x-z plane of the cross-section and a single B4 element positioned along the y-axis, which is the model's longitudinal axis. This three-dimensional model's spatial orientation and coordinates are depicted in Fig. 2. Two cross-ply stacking sequences have been selected, as detailed in Table 1. In these models, a 0° orientation indicates that the fibers are aligned parallel to the model's y-axis.
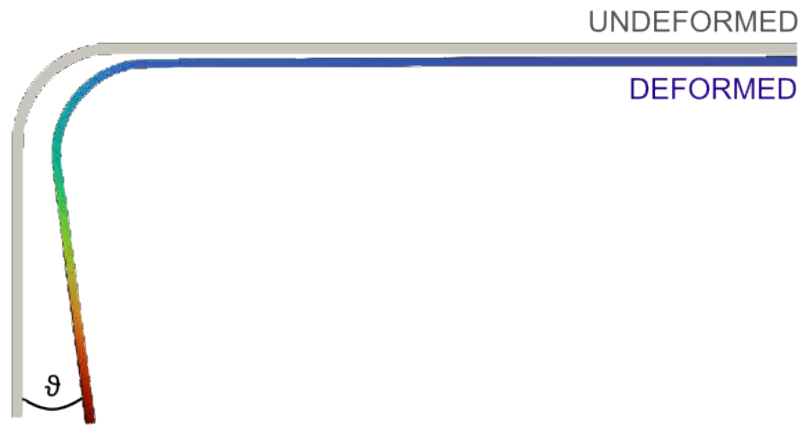
Figure 3 – Spring-in angle between the deformed and the undeformed model.

Table 1 – Cross-ply symmetrical and balanced stacking sequences.

ID LAM	Stacking sequence
1	$(0/90/0/90)_s$
2	$(90/0/90/0)_s$

4.1 Deformation analysis

Figure 4 shows the final deformation of the C-shaped model for LAM 1. Similar deformations were observed for LAM 2, making this visualization relevant to both cases. A similar deformation pattern was also observed in [13], where the maximum displacement occurs predominantly in the vertical flat parts and is uniformly distributed along the y-axis.
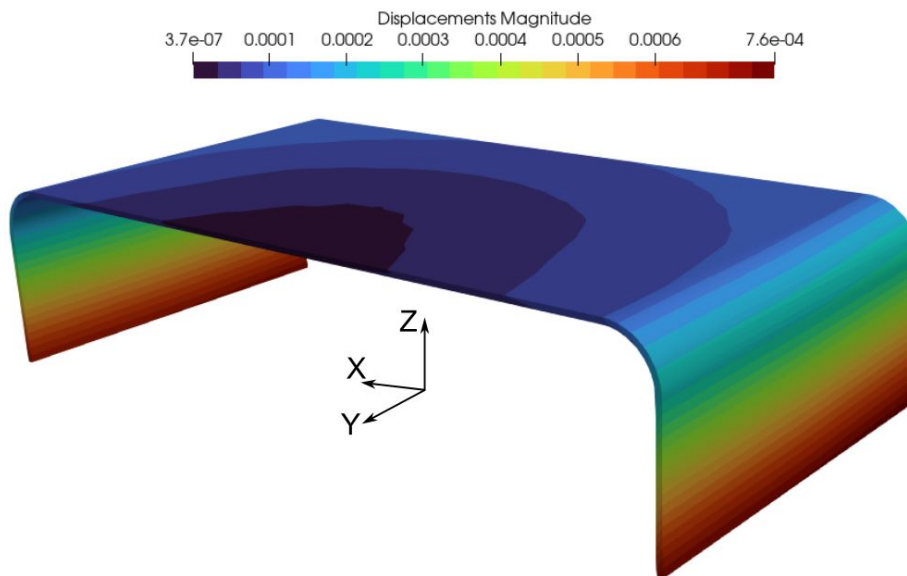

Figure 4 – Displacements of the C-shaped component with stacking sequence LAM 1.

Table 2 presents the maximum and minimum displacement values and maximum spring-in angles for the two cases under study. When these results are compared with those in [13], it is observed that for the same model and stacking sequence (LAM 1) but with a different material, the maximum displacement recorded was 8.48E-4 mm, leading to a spring-in angle of 1.34°. Altering the stacking sequence in that study did not significantly impact this angle. Similarly, the final spring-in angle for the two stacking sequences in this paper shows a slight variation. The comparatively higher values of displacement and spring-in angle in the referenced study [13] may be attributed to the lower tensile

Table 2 – Displacements and spring-in angles.

Stacking sequence	Min displ. [mm]	Max displ. [mm]	Max spring-in angle [°]
LAM 1	3.73E-7	7.55E-4	7.70E-01
LAM 2	4.71E-6	7.50E-4	7.40E-01

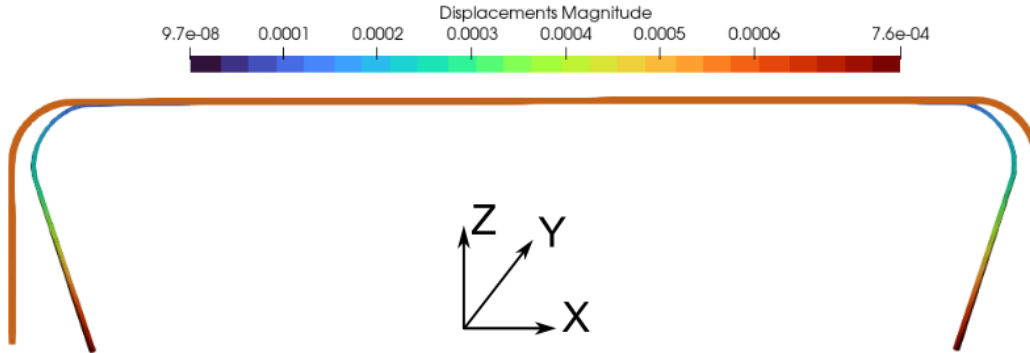strength of the matrix used.

Figure 5 – Change in shape of the model after the curing process for stacking sequence LAM 1.

Figure 5 depicts the deformation of the model within the x-z plane. The flange parallel to the x-axis remains parallel, while the two vertical flanges bend inwards.

4.2 Stress analysis

Figure 6 illustrates the two points selected for the stress evaluation. Specifically, σ_{xx} and σ_{yy} will be analyzed at x = 5 mm and x = 105 mm. These locations correspond to the model's center and the junction with the curved portion, respectively.
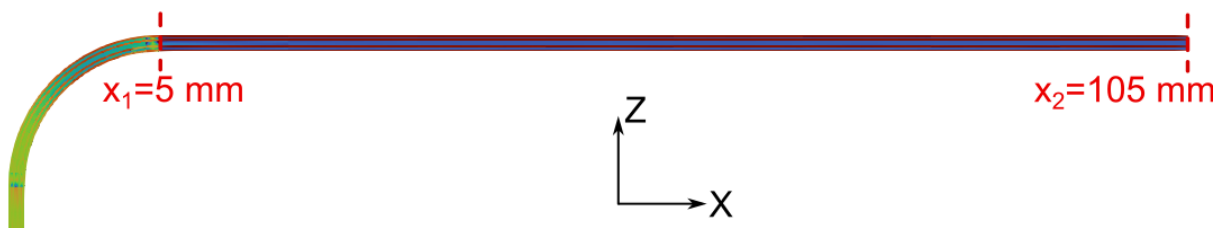

Figure 6 – Points where the through-the-thickness stress is evaluated.

The results in Fig. 7 show the through-the-thickness stress at location x_1. LAM 1 and LAM 2 exhibit similar stress values. Notably, in the case of σ_{xx}, layers oriented at 0° consistently show a state of tension, whereas those at 90° are in compression, a pattern consistent for both LAM 1 and 2. Conversely, the opposite behavior is evident for σ_{yy}. Figure 8 extends this analysis to x_2. Here, similar stress magnitudes are observed but with a more uniform distribution within each layer. This uniformity can be attributed to the flange being less affected by the curved section than in x_1.

5. Conclusions

This paper proposes a novel methodology for evaluating residual deformations and stresses in composite components during autoclave curing. The proposed approach is based on 1D structural theories with higher-order displacement fields within the CUF framework. Although 1D, the model can capture the 3D deformed state of the composite part and relative stress states. The results match qualitatively those from the literature and show significant values of residual stresses. Two symmetric and balanced stacking sequences were considered, and their influence on the results is marginal.
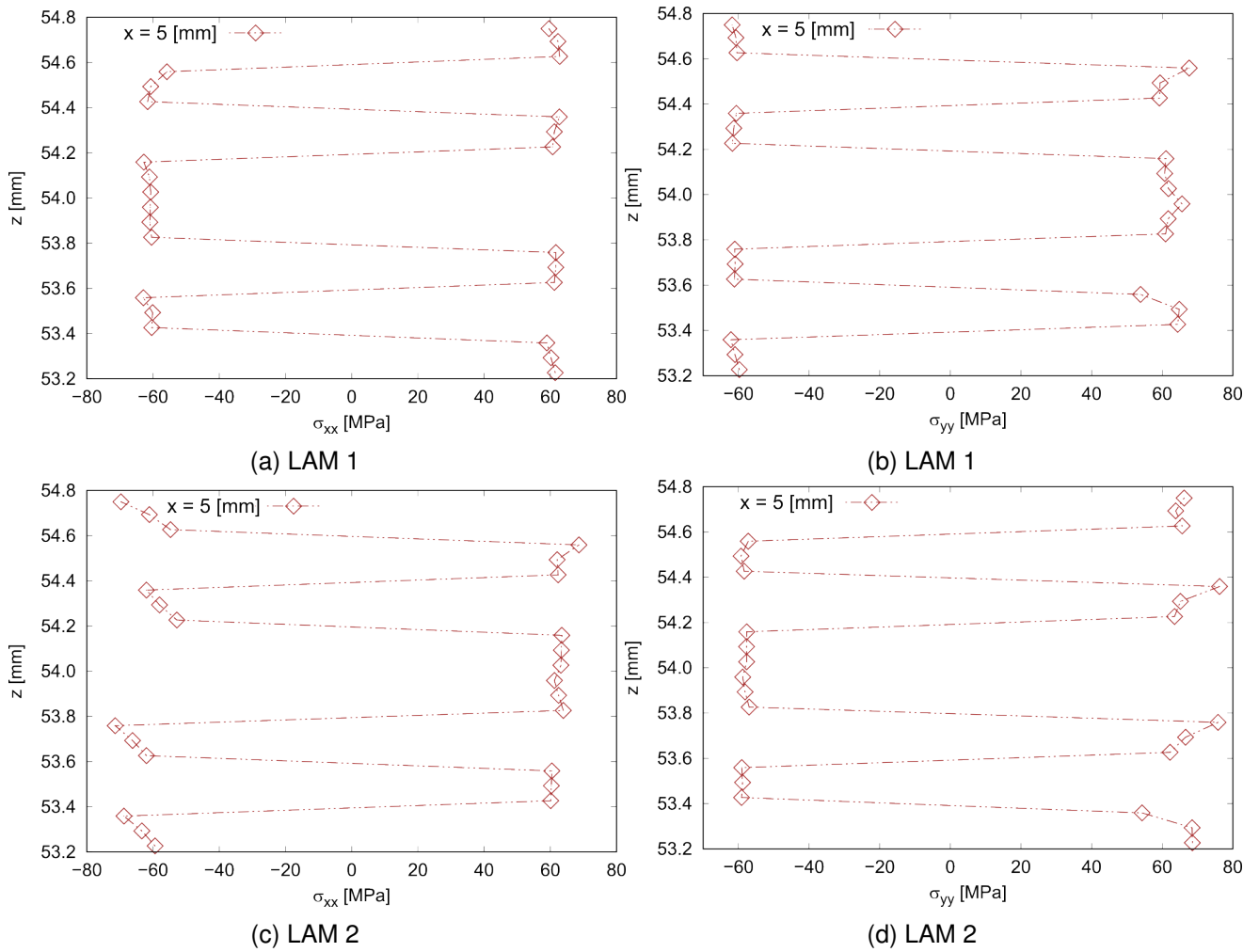
(a) LAM 1

(b) LAM 1

(c) LAM 2

(d) LAM 2

Figure 7 – Residual σ_{xx} and σ_{yy} in x_1.

(a) LAM 1

(b) LAM 1

(c) LAM 2

(d) LAM 2
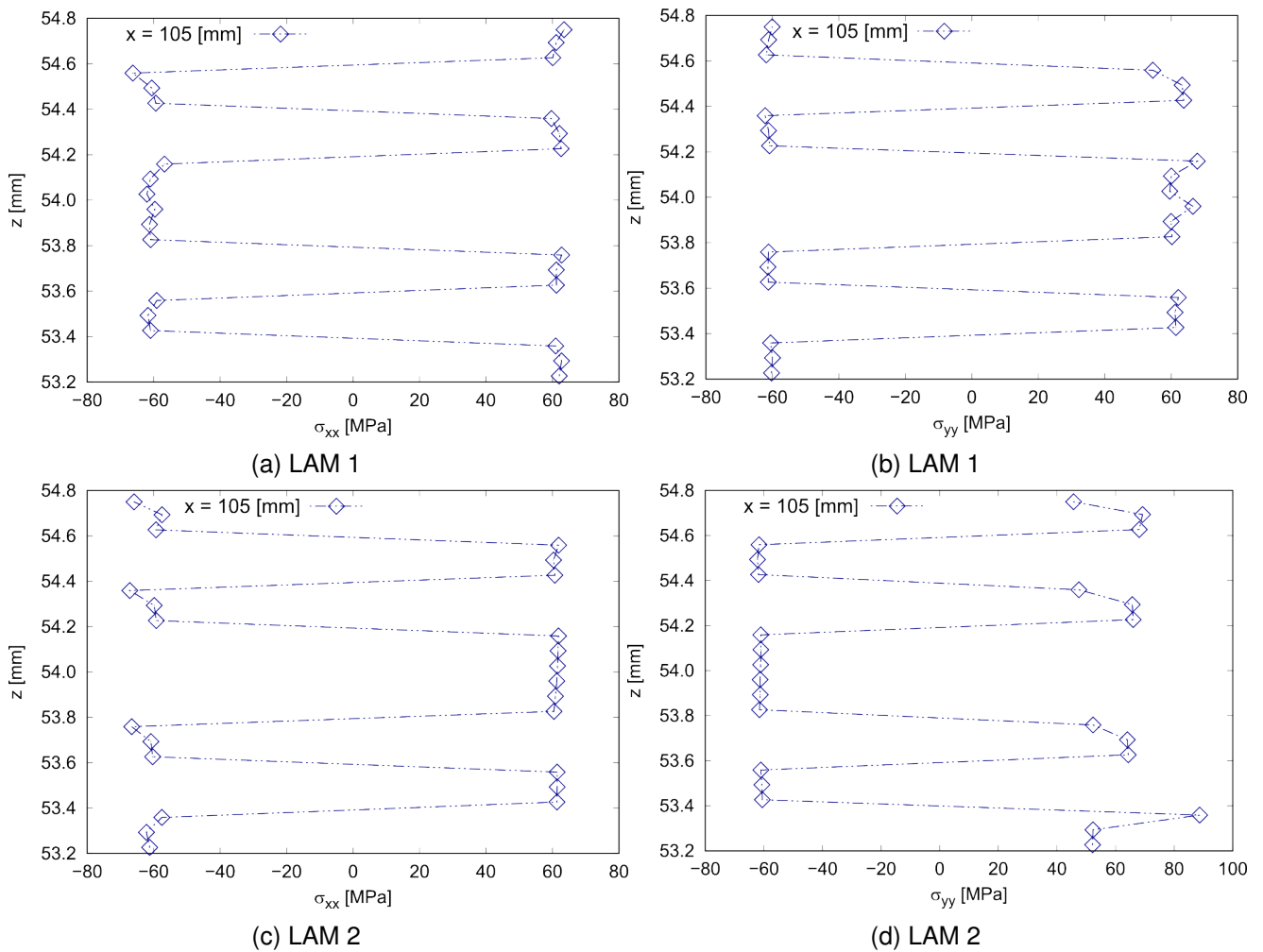
Figure 8 – Residual σ_{xx} and σ_{yy} in x_2.

6. Acknowledgements

7. Contact Author Email Address

The contact author email address is marco.petrolo@polito.it.

8. Copyright Statement

References

[1] Kesarwani S. *Polymer Composites in Aviation Sector*. International Journal of Engineering Research & Technology (IJERT), 2017

[2] Wang B, Fan S, Chen J, Yang W, Liu W, Li Y. *A review on prediction and control of curing process-induced deformation of continuous fiber-reinforced thermosetting composite structures*. Composites Part A: Applied Science and Manufacturing, 2023.

[3] Traiforos N, Matveev M, Chronopoulos D, Turner T. *Spring-in of composite L-shape specimens: An experimental and numerical investigation*. Composite Structures, 2023.

[4] Taranu G, Toma I O. *Experimental Investigation and Numerical Simulation of C-Shape Thin-Walled Steel Profile Joints.* Buildings, 2021.

[5] Hu W, Wang F, Cao D, Chen J, Feng J. *Quantitative validation of the analytical mode shapes of a beam-like structure with a Z-shaped configuration.* Journal of Mechanical Science and Technology, 2019

[6] Johnston A A. *An Integrated Model of the development of Process-Induced Deformation in Autoclave Processing of Composite Structures.* The University of British Columbia, 1997.

[7] Fernlund G, Mobuchon C, Zobeiry N. *Autoclave Processing.* Reference Module in Materials Science and Materials Engineering, 2017.

[8] Carrera E, Cinefra M, Petrolo M, Zappino E. *Finite Element Analysis of Structures through Unified Formulation.* John Wiley and Sons, Ltd, Hoboken, New Jersey, USA, 2014.

[9] Scano D, Carrera E, Petrolo M, *Use of the 3D Equilibrium Equations in the Free-Edge Analyses for Laminated Structures with the Variable Kinematics Approach.* Aerotecnica Missili e Spazio, 103, 179–195, 2024.

[10] Pagani A, Racionero Sanchèz Majano A, Zamani D, Petrolo M, Carrera E *Fundamental Frequency Layer-Wise Optimization of Tow-Steered Composites Considering Gaps and Overlaps.* Aerotecnica Missili e Spazio, In Press.

[11] Hexcel, HexPly 8552 product data sheet, 2016.

[12] Hexcel, HexTow AS4 product data sheet.

[13] Tang W, Xu Y, Hui X, Zhang W. *Multi-Objective Optimization of Curing Profile for Autoclave Processed Composites: Simultaneous Control of Curing Time and Process-Induced Defects.* Polymers 2022, 14, 2815.

[14] Hexcel, HexPly 3501-6 product data sheet, 2020.